Since January 2020 Elsevier has created a COVID-19 resource centre with free information in English and Mandarin on the novel coronavirus COVID-19. The COVID-19 resource centre is hosted on Elsevier Connect, the company's public news and information website.

Clinical Nutrition xxx (xxxx) xxx

Contents lists available at ScienceDirect

Clinical Nutrition

journal homepage: http://www.elsevier.com/locate/clnu

Covid-19

Myosteatosis predicting risk of transition to severe COVID-19 infection

Xiaoping Yi [a, 1], Haipeng Liu [a, 1], Liping Zhu [a, 1], Dongcui Wang [a], Fangfang Xie [a], Linbo Shi [b], Ji Mei [c], Xiaolong Jiang [d], Qiuhua Zeng [e], Pingfeng Hu [f], Yihui Li [g], Peipei Pang [h], Jie Liu [d], Wanxiang Peng [g], Harrison X. Bai [i], Weihua Liao [a, j, k, *], Bihong T. Chen [l]

[a] Department of Radiology, Xiangya Hospital, Central South University, Changsha, Hunan, 410008, PR China
[b] Department of Radiology, Yongzhou Central Hospital, Yongzhou, Hunan, 425006, PR China
[c] Department of Radiology, Changde Second People's Hospital, Changde, Hunan, 415001, PR China
[d] Department of Radiology, Affiliated Nan Hua Hospital, University of South China, Hengyang, Hunan, 421002, PR China
[e] Department of Radiology, Loudi Central Hospital, Loudi, Hunan, 417000, PR China
[f] Department of Radiology, Chenzhou Second People's Hospital, Chenzhou, Hunan, 423000, PR China
[g] Department of Radiology, Zhuzhou Central Hospital, Zhuzhou, Hunan, 412002, PR China
[h] GE Healthcare, Hangzhou, 310000, PR China
[i] Department of Diagnostic Imaging, Rhode Island Hospital, Providence, RI, 02903, USA
[j] Molecular Imaging Research Center of Central South University, Changsha, 410008, PR China
[k] National Clinical Research Center for Geriatric Disorders, Xiangya Hospital, Changsha, 410008, PR China
[l] Department of Diagnostic Radiology, City of Hope National Medical Center, Duarte, CA, USA

ARTICLE INFO

Article history:
Received 4 February 2021
Accepted 28 May 2021

Keywords:
Myosteatosis
Body composition
Predictive modeling
Transition risk
Coronavirus disease 2019 (COVID-19)

SUMMARY

Background: About 10–20% of patients with Coronavirus disease 2019 (COVID-19) infection progressed to severe illness within a week or so after initially diagnosed as mild infection. Identification of this subgroup of patients was crucial for early aggressive intervention to improve survival. The purpose of this study was to evaluate whether computer tomography (CT) - derived measurements of body composition such as myosteatosis indicating fat deposition inside the muscles could be used to predict the risk of transition to severe illness in patients with initial diagnosis of mild COVID-19 infection.
Methods: Patients with laboratory-confirmed COVID-19 infection presenting initially as having the mild common-subtype illness were retrospectively recruited between January 21, 2020 and February 19, 2020. CT-derived body composition measurements were obtained from the initial chest CT images at the level of the twelfth thoracic vertebra (T12) and were used to build models to predict the risk of transition. A myosteatosis nomogram was constructed using multivariate logistic regression incorporating both clinical variables and myosteatosis measurements. The performance of the prediction models was assessed by receiver operating characteristic (ROC) curve including the area under the curve (AUC). The performance of the nomogram was evaluated by discrimination, calibration curve, and decision curve.
Results: A total of 234 patients were included in this study. Thirty-one of the enrolled patients transitioned to severe illness. Myosteatosis measurements including SM-RA (skeletal muscle radiation attenuation) and SMFI (skeletal muscle fat index) score fitted with SMFI, age and gender, were significantly associated with risk of transition for both the training and validation cohorts ($P < 0.01$). The nomogram combining the SM-RA, SMFI score and clinical model improved prediction for the transition risk with an AUC of 0.85 [95% CI, 0.75 to 0.95] for the training cohort and 0.84 [95% CI, 0.71 to 0.97] for the validation cohort, as compared to the nomogram of the clinical model with AUC of 0.75 and 0.74 for the training and validation cohorts respectively. Favorable clinical utility was observed using decision curve analysis.

Abbreviations: COVID-19, Coronavirus disease 2019; MuLBSTA score, Multilobular infiltration, hypo-Lymphocytosis, Bacterial coinfection, Smoking history, hyper-Tension and Age Score; CRP, C-reaction protein; CK, Creatine kinase; LDH, Lactate dehydrogenase; SM-RA, Skeletal muscle radiation attenuation; SMFI, Skeletal muscle fat index; AST, Aspartate transferase; SMI, Skeletal muscle index.

* Corresponding author. Department of Radiology, Xiangya Hospital, Central South University, No. 87 Xiangya Road, Changsha 410008, PR China. Fax: +011 86 731 84327438.
E-mail address: Owenliao@csu.edu.cn (W. Liao).

[1] These authors contributed equally.

https://doi.org/10.1016/j.clnu.2021.05.031

Conclusion: We found CT-derived measurements of thoracic myosteatosis to be associated with higher risk of transition to severe illness in patients affected by COVID-19 who presented initially as having the mild common-subtype infection. Our study showed the relevance of skeletal muscle examination in the overall assessment of disease progression and prognosis of patients with COVID-19 infection.

1. Introduction

Coronavirus disease 2019 (COVID-19) has affected millions of patients causing a pandemic worldwide and has overwhelmed the health care capacity [1–6]. COVID-19 has caused varying severity of illness among the individuals affected by this viral infection [7–10]. The Chinese Management Guideline for COVID-19 indicated four subtypes of infection including light, common, severe and critical subtypes according to the severity of the infection ranging from mild to severe illness [11]. Patients with mild illness and common subtypes of the COVID-19 infection presented with mild to moderate symptoms of respiratory infection including fever and cough and most patients with mild illness had relatively good prognosis [8]. However, about 10–20% of patients would ultimately progress to severe illness including both the severe and critical subtypes during a period of about 3–10 days after initial diagnosis as having the mild illness, resulting in mortality rates ranging from 30% to 50% [6,7,9,10,12,13]. Considering the relative lack of effective treatment and demand for intensive care for patients with severe illness [6,14,15], early identification of patients with COVID-19 who would transition to severe illness would be essential for formulating treatment plan and informing on prognosis.

Prior studies have identified several risk factors associated with disease severity and high risk of death in patients with COVID-19, including age, a higher MuLBSTA score (Multilobular infiltration, hypo-Lymphocytosis, Bacterial coinfection, Smoking history, hyper-Tension and Age Score) [9,16], the presence of viral RNA in the blood [17], and abnormally expressed cytokines such as c-reaction protein (CRP), creatine kinase (CK) and lactate dehydrogenase (LDH) [3,7–10,12,18]. However, because of the overlap of these clinical factors between patients with the mild illness and those with severe illness, none of the identified risk factors could effectively predict the risk of transition to severe illness in individual patients with COVID-19, especially when the illness was at an early stage with limited available clinical information. There is an unmet need to identify the transition risk at an early stage to facilitate aggressive treatment for those with high risk for developing severe illness.

Myosteatosis indicating fat deposition inside the muscles is defined as abnormal distribution of inter and intra-myocellular adipose tissue, which is related to reduced muscle quality, physical fitness and muscle function [19–21]. Computed tomography (CT) is one of common methods for accessing myosteatosis with a radiological marker termed skeletal muscle radiation attenuation (SM-RA) [21–23]. Cumulative evidence suggests that myosteatosis is associated with susceptibility, severity, and prognosis of a variety of conditions such as cancer, aging, sarcopenia [19,22–29] and viral pneumonia [30]. However, there is still a paucity of knowledge regarding the clinical impact of pre-treatment baseline body composition assessment such as CT-derived myosteatosis in patients with COVID-19.

The current study assessed myosteatosis on the archived chest CT images acquired as part of work up for COVID-19 infection for patients during the initial outpatient clinical visit. We hypothesize that the CT-derived measurements of myosteatosis could be effective in predicting the risk of transition to severe illness in patients with COVID-19 who presented as the mild common-subtype COVID-19 infection. Identifying the patients with high risk of transition to severe COVID-19 infection should be helpful in assisting clinical decision making and in prioritizing aggressive treatment for those who may progress to severe illness.

2. Materials and methods

2.1. Study design and participants

Patients with laboratory-confirmed COVID-19 infection presenting initially as having the mild common-subtype illness at admission between Jan 21, 2020 and Feb 19, 2020 were retrospectively identified from the six designated hospitals for treating patients with COVID-19 in Hunan province, P.R. China. Reverse-transcription polymerase chain reaction (RT-PCR) assays for laboratory confirmation of severe acute respiratory syndrome coronavirus 2 (SARS-CoV-2) were performed in accordance with the World Health Organization (WHO) guidance [31]. CT-derived myosteatosis measurements such as skeletal muscle radiation attenuation (SM-RA) were obtained from the initial chest CT images at the level of the twelfth thoracic vertebra (T12) and were used to build models to predict the risk of transition. Details of the patient recruiting process and exclusion criteria were shown in Fig. 1. Information on the six participating hospitals was presented in Supplementary Table 1.

The illness severity of COVID-19 was defined according to the Chinese Management Guideline for COVID-19 (version 7.0) [11], which indicated four subtypes of infection including light, common, severe and critical subtypes ranging from the mild to severe illness. Results (positive or negative) of laboratory tests of blood were made based on cut-off values of the testing equipment.

This multicenter retrospective study was approved by the Institutional Review Board (IRB) in all participating hospitals (IRB#: 202002019), and written informed consents were waived due to the retrospective nature of this study.

2.2. Data collection

Information on the demographics, clinical data, laboratory values, outcome data and chest CT images were abstracted from medical records. We only included the available data prior to hospital admission for analysis. This data was reviewed by two clinicians (L.Z and F.X) and a third researcher (X.Y) adjudicated any difference in interpretation between the two primary reviewers.

2.3. Chest CT image analysis and body composition measurement

Patients' chest CT images acquired during the initial outpatient clinical visit prior to or at admission were retrieved from the hospitals' Picture Archiving and Communication Systems (PACS, Carestream, Canada). The time span between the chest CT scans and the confirmed COVID-19 infection was 6 hours to 4 days as some patients underwent repeated pharyngeal swab nucleic acid

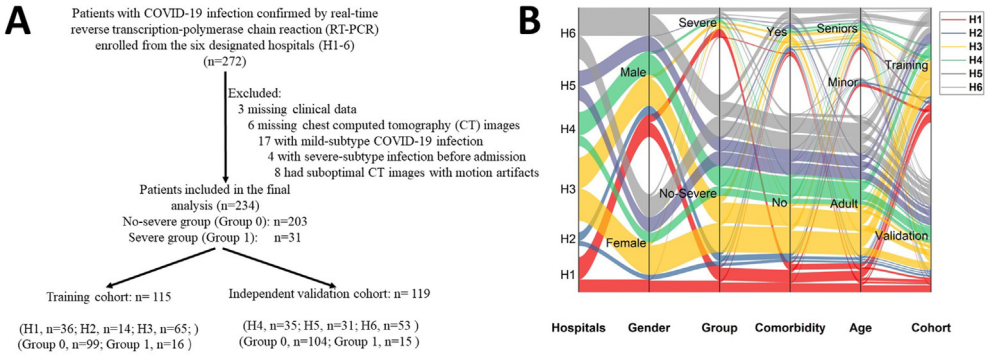

Fig. 1. Study enrollment and cluster projections of patients with COVID-19 (A) Flow-chart demonstrating the patients' recruiting process (B) Sankey diagram showing the scmap cluster projections of the patients with COVID-19 in the six designated hospitals (H1−H6), gender/age composition, and case severity distribution.

tests for confirmation of COVID-19 infection. All axial CT images were reconstructed to a thickness of 3 mm. Detailed information on the chest CT scanning protocols were included in Supplementary Table 2.

One axial unenhanced image from each chest CT scan at the level of the twelfth thoracic vertebra level (T12) was selected. The chest/abdominal wall and back muscles including the psoas, paraspinal, transversus abdominis, rectus abdominis, internal oblique muscles, and external oblique muscles were manually segmented on the selected axial image for each scan. Body composition measurements were performed on the segmented image using a workstation (Advantage Windows workstation 4.6, GE Healthcare, Milwaukee, Wisconsin, USA).

Multiple parameters for body composition including the skeletal muscle area (SMA) (−29−150Hu), septocutaneous muscle fat area (SMFA) (−190~-30Hu), myosteatosis area (MyoA) (−30−30Hu), skeletal muscle radiation attenuation (SM-RA), proportion of skeleton muscle fat (PSMF), proportion of myosteatosis muscle (Pmyo), proportion of skeleton muscle (PSM), and mean CT value of myosteatosis muscle (CT_Myo) were measured in a similar method as previously reported in literature [22,23]. In addition, additional parameters including the skeletal muscle index (SMI) and septocutaneous muscle fat index (SMFI) were calculated by normalizing the measured muscle area to the square vertical length from the anterior edge of the first thoracic vertebra to the anterior superior edge of the tenth thoracic vertebra on the CT images (cm^2/m^2). The ratio of the volume of lung lesions including overall lesion, ground-glass opacity and consolidation, to the volume of the entire lung was measured using Intelligent Evaluation System of Chest CT for COVID-19 (YITU Healthcare, Shanghai, China). CT image analysis and prediction modeling were presented in Fig. 2.

Since there were no established cutoff values based on T12 level measurements for diagnosing thoracic myosteatosis in the literature, we therefore identified our own cut-off values for myosteatosis for the T12-muscle-index in a similar approach as other researchers for a similar cohort size [22,23,32]. Given the modest sample size of our cohort that might be insufficient for cut-point analysis through optimal stratification, we determined our cut-off values based on tertiles stratified by gender. This method was more reasonable for comparison between groups, especially for subjects with lower/higher values or values around the cutoff. Cut-off values were set at the lowest tertile of SMI and SM-RA for diagnosing myosteatosis [22,23,32].

2.4. Reproducibility of CT body composition measurements

Two radiologists performed their independent segmentations of 30 randomly chosen patients' chest CT images. The inter-observer (reader 1 versus reader 2) and intra-observer (reader 1 twice) correlation coefficient (ICC) values were evaluated. The final consistency was evaluated by the following criteria applied to the ICC value: less than 0.20 indicating poor reproducibility, 0.21−0.40 indicating fair reproducibility, 0.40−0.60 indicating moderate reproducibility, 0.61−0.80 indicating good reproducibility and 0.81−1.00 indicating excellent reproducibility. The inter-observer ICCs of CT body composition measurements between reader 1 (first time) and reader 2 ranged from 0.951 to 1.000. The intra-observer ICC of reader 1's two measurements ranged from 0.981 to 1.000. As a result, the body composition measurements obtained by reader 1 were used in the subsequent data analysis.

2.5. Development of an individualized prediction model

Patients (n = 234) were randomly assigned to the training cohort (n = 118) and the independent validation cohort (n = 116) with a 1:1 ratio. The univariate logistic regression analysis in the training cohort was performed to determine the association between myosteatosis and clinical/laboratory variables, and the risk of transition to severe illness. Candidate predictors were selected from the univariate analysis ($P < 0.05$) and then underwent multivariate logistic regression using the likelihood ratio test, with Akaike's information criterion (AIC) as the stopping rule to select the correlated factors. The minimums of the AIC corresponded to the optimal combination of factors. Considering the potential association among SMFI, age and gender, a new factor termed SMFI score was fitted based on these three factors. A model for predicting risk of transition to severe illness based on clinical data without myosteatosis parameters was constructed. Subsequently, a new model combining the myosteatosis parameters with the clinical model was developed. A nomogram was generated to provide the clinicians with a quantitative tool to predict individual probability of the transition risk. Comparison of the performance data for the two models was performed.

2.6. Model performance and nomogram validation

The calibration of the nomogram was evaluated by calibration curves (Hosmer−Lemeshow H test), and the diagnostic efficiency was evaluated with the receiver operating characteristic (ROC) curve. The performance of nomogram was tested in the validation cohort. Using the logistic regression formula established in the training cohort, the total points for each patient in the validation cohort were calculated, and the area under the curve (AUC) and calibration curve were derived. To estimate the prediction error, we tested the proposed model further using a 1000-iteration bootstrap analysis for both the training and validation cohorts. For each

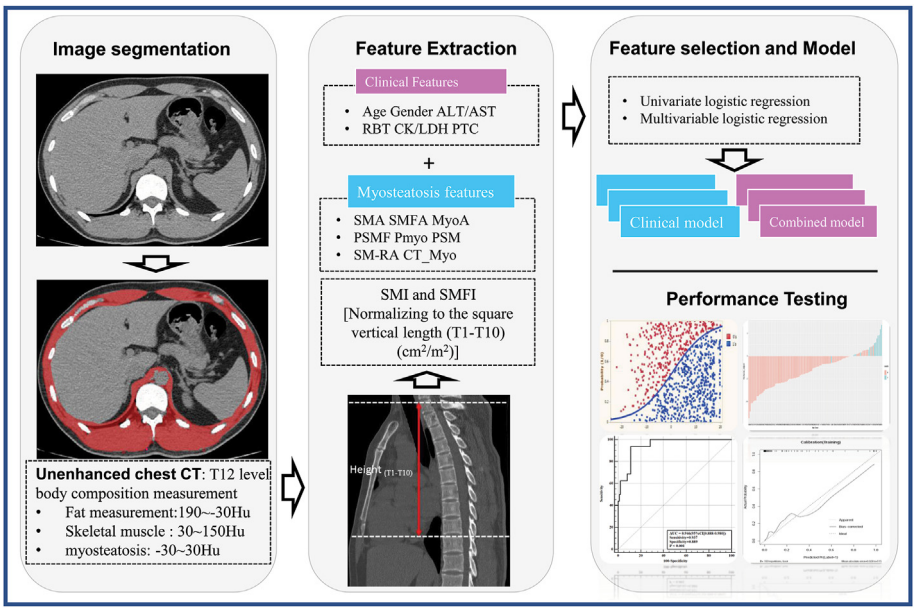

Fig. 2. Workflow of data analysis including chest CT image segmentation, clinical/myosteatosis feature selection, model building and performance testing. Abbreviations: SMA, skeletal muscle area; SMFA, septocutaneous muscle fat area; MyoA, myosteatosis area; PSMF, proportion of skeleton muscle fat; Pmyo, proportion of myosteatosis muscle; PSM, proportion of skeleton muscle, SM-RA, skeletal muscle radiation attenuation; CT_Myo, mean CT value of myosteatosis muscle; SMI, skeletal muscle index; SMFI, septocutaneous muscle fat index; LR, Logistic regression; ALT, alanine aminotransferase; AST, aspartate transferase; RBT, Routine blood test; CK, creatine kinase; LDH, lactate dehydrogenase; PTC/PCT, Procalcitonin.

repetition, a random subset of 70% patients from the training or the validation cohort was selected and the corresponding AUC values were calculated. Decision curve analysis was performed to evaluate the clinical usefulness of the nomogram in the validation cohort.

2.7. Statistical analysis

All statistical analysis was conducted with R software (version 3.5.2; http://www.Rproject.org). Univariate analysis for clinical features was implemented by Chi-square test (categorical variable) or Mann–Whitney U test (continuous variable), as appropriate to compare differences between the patients with severe illness and the patients with no-severe illness. Nomogram construction and calibration plots were performed using the "rms" package of R software. The statistical significance levels were all two-sided with statistical significance set at 0.05.

3. Results

3.1. Patient characteristics

A total of 234 patients with COVID-19 who presented initially having the mild common-subtype infection were included in this study and 31 of them transitioned to severe illness during hospitalization. All patients were randomly assigned to the training cohort (n = 118) and the validation cohort (n = 116) at a 1: 1 ratio (Fig. 1).

Patient characteristics for both cohorts and the comparison between the patients with severe illness and the patients with no-severe illness were presented in Table 1. Significant differences between the cohorts were found for male patient's age (P = 0.001), symptom including dyspnea and diarrhea (P < 0.05), comorbidities including coronary heart disease, diabetes mellitus, hypertension and chronic obstructive pulmonary disease (COPD) (all P < 0.05), physiological measures of oxygen saturation (SpO_2), laboratory markers including aspartate transferase (AST), creatine kinase (CK), C-reactive protein (CRP), D-dimmer and procalcitonin (all P < 0.05) (Table 1). There were no statistical differences (P > 0.05) between the training cohort and the validation cohorts in the clinical variables, indicating a reasonable classification.

3.2. Comparison of myosteatosis measurements between the patients with severe and no-severe illness

The characteristics for both severe and no-severe cohorts were shown in Table 1. When compared to the no-severe cohort, the patients with severe illness showed significantly higher SMFI and higher incidence of myosteatosis with P < 0.05 (Table 1).

3.3. Identifying risk factors for transition to severe illness

In univariate analysis, myosteatosis (reduced SM-RA), sarcopenia (reduced SMI), age, lymphopenia, leukocytosis, reduced SpO_2 (less than 96%), and elevated values of CRP, CK and AST, d-dimer, and procalcitonin were also associated with higher risk of transition to severe illness (Supplementary Table 3). Multivariate logistic regression analysis showed that the reduced SM-RA, SPO_2 (<96%), and elevated values of CRP, CK and SMFI-score were independent predictors for transition to severe illness (Supplementary Fig. 1).

3.4. Prediction model performance

The clinical model built with the SPO_2, CRP and CK achieved a modest efficiency with an AUC of 0.75 (95% CI:0.63–0.88) for the training cohort, and 0.74 (95%CI: 0.61–0.88) for the validation cohort, respectively. After addition of the CT-derived myosteatosis measurements to the clinical model, the prediction performance of the combined model was significantly improved (Delong test, P = 0.002 for the training cohort versus P = 0.04 for the validation cohort), with an AUC of 0.85 (95%CI: 0.75–0.95) for the training cohort and 0.84 (95%CI: 0.71–0.97) for the validation cohort, as well

Table 1
Demographic, clinical, laboratory, and chest CT findings of patients with COVID-19 included in the study.

Characteristic	Total (n = 234)	Patients with severe illness (n = 31)	Patients with no-severe illness (n = 203)	P Value[a]	Training Cohort (n = 118)	Validation Cohort (n = 116)	P Value[b]
Demographics and clinical characteristics							
Gender				0.057			0.184
Male	133 (56.8)	23 (74.2)	110 (54.2)	•••••••	43 (36.4)	58 (50.0)	•••••••
Female	101 (43.2)	8 (25.8)	93 (45.8)	•••••••	75 (63.6)	58 (50.0)	•••••••
Age (y)[#]							
Male	41.0 (5.0−80.0)	56 (26−80)	40 (5.0−75.0)	0.775	40.0 (5.0−80.0)	46.0 (7.0−75.0)	0.533
Female	47.0 (2.0−81.0)	54.5 (33.0−76.0)	45.0 (2.0−81.0)	0.629	50.0 (22.0−81.0)	45.0 (2.0−74.0)	0.096
Both	44.5 (2.0−81.0)	45.0 (26.0−80.0)	43.0 (2.0−81.0)	0.001**	43.0 (5.0−81.0)	45.5 (2−75.0)	0.119
Comorbidity							
Coronary heart disease	5 (2.1)	3 (9.7)	2 (1.0)	0.014*	1 (0.8)	4 (3.4)	0.356
Diabetes	18 (7.7)	7 (22.6)	11 (5.4)	0.003**	9 (7.6)	9 (7.8)	1.000
Hypertension	25 (10.7)	7 (22.6)	18 (8.9)	0.047*	11 (9.3)	14 (12.1)	0.639
COPD	7 (3.0)	4 (12.9)	3 (1.5)	0.004**	2 (1.7)	5 (4.3)	0.429
Chronic liver disease	9 (3.8)	0 (0.0)	9 (4.4)	0.488	5 (4.2)	4 (3.4)	1.000
Chronic kidney disease	0 (0.0)	0 (0.0)	0 (0.0)	•••••••	0 (0.0)	0 (0.0)	•••••••
Cancer	4 (1.7)	1 (3.2)	3 (1.5)	1.000	2 (1.7)	2 (1.7)	1.000
Overall comorbidity							
1 and more comorbidity	50 (21.4)	12 (38.7)	38 (18.7)	0.022*	24 (20.3)	26 (22.4)	0.820
2 and more comorbidity	13 (5.6)	6 (19.4)	7 (3.4)	0.001*	5 (4.2)	8 (6.9)	0.547
Disease							
Fever (>37.5C) (n, %)	164 (50.4)	25 (80.6)	139 (68.5)	0.243	82 (69.5)	82 (70.7)	0.954
cough	163 (69.7)	26 (83.9)	137 (67.5)	0.101	84 (71.2)	79 (68.1)	0.711
Dyspnea	25 (10.7)	7 (22.6)	18 (8.9)	0.047*	14 (11.9)	11 (9.5)	0.705
Myalgia	18 (7.7)	2 (6.5)	16 (7.9)	1.000	6 (5.1)	12 (10.3)	0.206
Fatigue	58 (24.8)	6 (19.4)	52 (25.6)	0.597	33 (28.0)	25 (21.6)	0.325
Headache	31 (13.2)	2 (6.5)	29 (14.3)	0.361	13 (11.0)	18 (15.5)	0.411
Nausea and/or vomiting	16 (6.8)	3 (9.7)	13 (6.4)	0.771	9 (7.6)	7 (6.0)	0.823
Diarrhea	19 (8.1)	7 (22.6)	12 (5.9)	0.005**	7 (5.9)	12 (10.3)	0.319
Asymptomatic	22 (9.4)	1 (3.2)	21 (10.3)	0.350	12 (10.2)	10 (8.6)	0.856
SPO2 (<96%)	31 (13.2)	11 (35.5)	20 (9.9)	<0.001**	17 (14.4)	14 (12.1)	0.738
Time from illness onset to out-patients (days)	3.0 (0.0−19.0)	4.6 (3.4)	4.1 (3.5)	0.464	4.3 (3.5)	4.1 (3.4)	0.656
Time from illness onset to hospital admission (days)	5.0 (0.0−20.0)	6.2 (3.3)	5.9 (4.1)	0.688	5.6 (3.8)	6.2 (4.2)	0.283
Laboratory findings							
White blood cell count, × 10^9 per L				0.147			0.863
<4	90 (38.4)	12 (38.7)	78 (38.4)	•••••••	44 (37.3)	46 (39.7)	•••••••
4−10	131 (56.0)	15 (48.4)	116 (57.1)	•••••••	68 (57.6)	63 (54.3)	•••••••
>10	13 (5.6)	4 (12.9)	9 (4.4)	•••••••	6 (5.2)	7 (6.0)	•••••••
Lymphocyte count × 10^9 per L							
<0.8	45 (19.2)	8 (25.8)	37 (18.2)	0.452	25 (21.2)	20 (17.2)	0.549
ALT (>40)	44 (18.8)	8 (25.8)	36 (17.7)	0.410	21 (17.8)	23 (19.8)	0.818
AST (>40)	31 (13.2)	11 (35.5)	20 (9.9)	<0.001**	18 (15.3)	13 (11.2)	0.471
Lactate dehydrogenase (elevated)	136 (58.1)	10 (32.3)	88 (43.3)	0.332	74 (62.7)	62 (53.4)	0.192
CRP	100 (42.7)	23 (74.2)	77 (37.9)	<0.001**	49 (41.5)	51 (44.0)	0.806
Creatine kinase (elevated)	34 (14.5)	9 (29.0)	25 (12.3)	0.029*	20 (16.9)	14 (12.1)	0.382
D-dimer (elevated)	61 (26.1)	14 (45.2)	47 (23.2)	0.0173**	31 (26.3)	30 (25.9)	1.000
Procalcitonin	30 (12.8)	8 (25.8)	22 (10.8)	0.02**	17 (14.4)	13 (11.2)	0.172
CT chest imaging findings							
Lesion type							
Consolidation	163 (69.7)	26 (83.9)	137 (67.5)	0.065	76 (64.4)	87 (75.0)	0.078
Ground-glass opacity	231 (98.7)	31 (100)	200 (98.5)	0.496	117 (99.2)	114 (98.3)	0.551
Reticular or stripe	131 (56.0)	25 (80.6)	117 (57.6)	0.015*	71 (60.2)	71 (61.2)	0.871
Bilateral pulmonary infiltration	195 (83.3)	31 (100)	164 (80.8)	0.008**	98 (83.1)	97 (83.6)	0.907
Multi-lobe infiltration	187 (77.0)	30 (96.8)	157 (77.3)	0.012*	95 (80.5)	92 (79.3)	0.819
Proportion of lesion volume to whole lung							
Overall lesions	8.56 (0.02−71.96)	20.08 (1.26−71.96)	6.95 (0.02−66.48)	0.801	8.56 (0.02−71.96)	8.65 (0.02−50.94)	0.528
Ground-glass opacity	6.86 (0.01−59.65)	16.90 (1.10−55.43)	5.84 (0.01−59.65)	0.834	6.91 (0.02−59.65)	6.83 (0.01−43.45)	0.536
Consolidation	1.13 (0.0−27.92)	3.15 (0.15−27.92)	0.88 (0.00−15.93)	0.569	0.91 (0.00−27.92)	1.51 (0.00−15.93)	0.552
Body composition							
SMI	24.2 (15.3−40.2)	25.4 (20.5−40.2)	23.7 (15.3−37.3)	0.021*	24.8 (15.4−33.8)	23.7 (15.3−40.2)	0.273

(*continued on next page*)

Table 1 (*continued*)

Characteristic	Total (n = 234)	Patients with severe illness (n = 31)	Patients with no-severe illness (n = 203)	P Value[a]	Training Cohort (n = 118)	Validation Cohort (n = 116)	P Value[b]
SMFI	3.6 (0.2−11.9)	5.0 (1.3−10.9)	3.4 (0.2−11.9)	<0.001**	3.4 (0.20−10.9)	3.8 (0.61−11.9)	0.259
SM-RA	41.8 (26.8−60.2)	37.0 (27.1−53.1)	43.0 (26.8−60.2)	0.007**	43.1 (27.1−60.2)	40.8 (26.8−54.7)	0.184
Sarcopenia	•••••••	5 (16.1)	73 (36.0)	0.029*	37 (31.4)	41 (35.3)	0.518
Myosteatosis	•••••••	18 (58.1)	59 (29.1)	0.001**	34 (28.8)	43 (37.1)	0.179

Note. —Unless otherwise indicated, data are numbers of patients, and data in parentheses are percentages. # age is presented as median (minimum ~ maximum). P Value[a]: comparing the group with severe illness and the group with no-severe illness; P Value[b]: comparing between the training cohort and the validation cohort. The symbol * for $P < 0.05$ and the symbol ** for $P < 0.01$ suggest a significant difference between the severe group and the no-severe group. Abbreviations: COPD, chronic obstructive pulmonary disease; ALT, alanine aminotransferase; AST, aspartate transferase; CRP, c-reaction protein; SMI, skeletal muscle index; SMFI, Skeletal muscle fat index; SM-RA, skeletal muscle radiation attenuation.

as a good performance of consistence (bootstrap, Training cohort: 0.85 ± 0.04; Validation cohort: 0.84 ± 0.03) (Figs. 3A, B and 3C).

In order to evaluate the impact of diabetes on disease progression in COVID-19 infection, we added diabetes into the final logistic regression model. Our adjusted model with addition of diabetes as a risk factor for differentiating patients with higher-risk of transition to severe disease performed similarly to the original model without diabetes, with AUC of 0.86 (95% CI: 0.77−0.95) and AUC of 0.85 (95% CI: 0.75−0.95) respectively (Supplementary Fig. 2). There were no significant differences in the performance of these two models with and without addition of diabetes as a predictor (Delong's test, P = 0.1239).

The calibration curve of the nomogram for the probability of transition to severe illness showed good agreement between prediction and observation for both cohorts (Fig. 3D, and E). The Hosmer−Lemeshow H test yielded a nonsignificant statistical evaluation for the training (P = 0.6802) cohort and the validation cohort (P = 0.481), suggesting no departure from perfect fit. The boost plots for myosteatosis nomograms were presented in Supplementary Fig. 3.

The decision curve analysis for the nomogram was presented in Fig. 4. The decision curve showed that if the threshold probability of a patient or a doctor was greater than 5%, using the nomogram to predict severe illness status in COVID-19 patients added more benefit than either the diagnose-all-patients scheme or the diagnose-none scheme. After exceeding the threshold of ~10%, the combined model showed more clinical benefits than the clinical model alone.

4. Discussion

In this study, we found CT-derived thoracic myosteatosis measurements to be independent predictors for progression to severe illness in patients with COVID-19 who were initially diagnosed as having the mild common-subtype infection. Our prediction model combining CT-derived myosteatosis measurements and the clinical laboratory data obtained from the first clinic visit showed satisfying performance in differentiating the patients with higher risk of transition to severe COVID-19 infection from those with lower risk of transition. In addition, our myosteatosis nomogram showed promising results to be used as a potential tool for assessing COVID-19 infection in clinical practice.

Our findings of thoracic myosteatosis predicting progression of COVID-19 infection were generally in line with prior studies regarding the adverse implication of myosteatosis. Published literature has shown that myosteatosis is positively associated with the increased severity of the patient's disease, longer hospital stays, more complications, earlier postoperative recurrence, and worse prognosis [19,21−25]. Recent studies have reported that myosteatosis was often associated with a weak physical state of the patients [20,21], and may contribute to an increased risk of developing severe symptoms [33] and viral pneumonia [24]. We

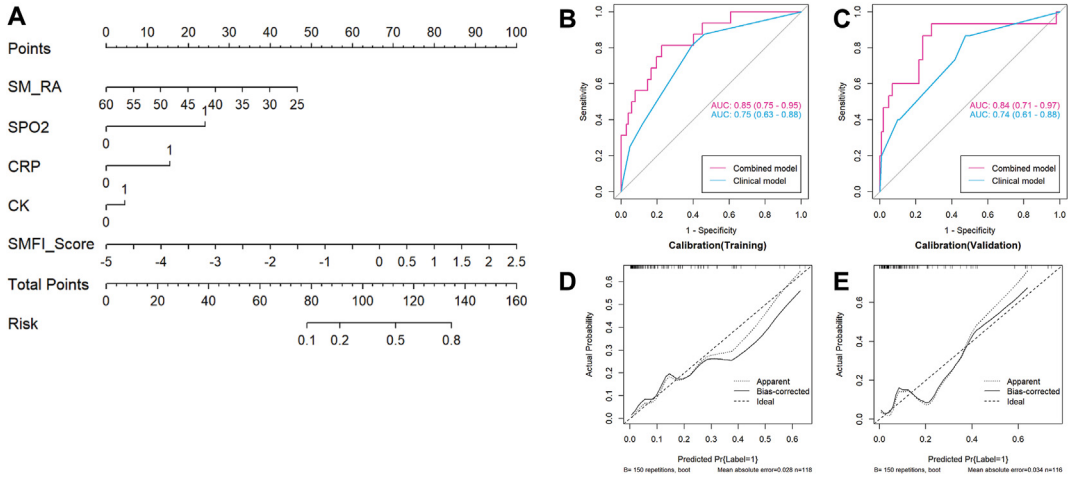

Fig. 3. Myosteatosis nomogram, ROC curves and calibration curves for predicting the risk of transition to severe illness (A) Myosteatosis nomogram developed in the training cohort (B) ROC curves for the training cohort (C) ROC curves for the independent validation cohort for both the clinical model and the combined model. Calibration curves of the myosteatosis nomogram for the training cohort (D) and for the validation cohort (E). Abbreviations: SM-RA, skeletal muscle radiation attenuation; SPO2, physiological measures of oxygen saturation; CRP, c-reactive protein; CK, creatine kinase; and SMFI-Score, septocutaneous muscle fat index score.

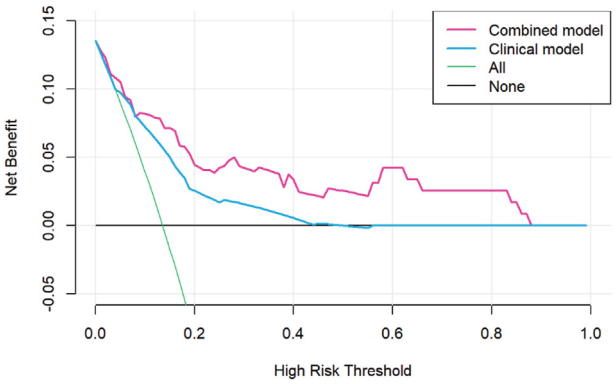

Fig. 4. Decision curve analysis of the myosteatosis nomograms for the combined model and the clinical model alone. The y-axis measures the net benefit. The blue line represents the decision curve for the clinical model. The pink line represents the decision curve for the combined model with addition of CT myosteatosis features to the clinical model. The black line represents the assumption that no patients had the risk if transition to severe illness and the green line represents all patients would transition to severe illness.

speculate that the patients with myosteatosis in our cohort implicated relatively poor physical fitness, thus being more susceptible to severe COVID-19 infection.

We found that patients in the group with severe illness not only had a higher rate of myosteatosis, but also had a higher SMFI value indicating more subcutaneous adipose tissue deposition in the thoracic muscles. Increased adipose tissue in the muscles has been related to obesity, which is an important underlying factor associated with myosteatosis [34]. The adverse impact of obesity on immune responses and infection such as viral influenza pneumonia has been reported [30,35]. Obesity could affect the immune response by regulating leptin, whose signaling plays an important role in virus-related adaptive immune response [36]. In addition, obesity promotes the activation of immune cells and increases the production of pro-inflammatory cytokines, which has been proposed as the underling mechanism for rapid transition to severe disease, multi-organ dysfunction, and even death in various diseases [36]. We therefore speculate that the patients progressing to severe illness may have underlying subclinical muscular atrophy and obesity as indicated by their higher SMFI values, predisposing them to severe COVID-19 infection.

The underlying pathophysiological mechanism regarding the association between myosteatosis and progression of COVID-19 infection is not clear. We speculate that myosteatosis with weakening thoracic muscle in our cohort may have resulted in a diminished effort for coughing, which may partly be responsible for disease progression. Coughing is the most direct protective mechanism against lung infections, requiring coordinated activation and movement of respiratory muscles and internal laryngeal muscles [22,37]. A prior study of healthy older men and women has showed that reduced muscle strength was significantly associated with decreased lung function, implying the inter-dependence between muscle strength and vital capacity lung function [38]. We hypothesize that myosteatosis with reduced muscle quality in our patients may have weaken the protective coughing mechanism against pneumonia, thus increasing the risk of transition to severe COVID-19 infection. Since most patients may have similar muscle mass, therefore diminished muscle quality rather than quantity as reflected by myosteatosis may have played a role in the transition to severe COVID-19 infection.

The satisfying performance of our prediction model may be due to incorporation of important clinical and laboratory variables such as age, SPO_2, and CK [7–10,39]. Our study results were consistent with others indicating these variables being relevant to COVID-19 infection. For example, age has been shown to be an important risk factor for poor prognosis in patients with COVID-19 and older patients tend to have more severe infection with higher mortality rate [7–9]. In addition, myosteatosis becomes more severe with the aging process [19,23,39,40]. Reduced SPO2 (<96%) usually suggests a significant impairment of lung exchange function and potential hypoxemia, which has been reported to be associated with severity of COVID-19 [12] and community acquired pneumonia [41]. We found a significant higher incidence of reduced SPO_2 in patients with more severe COVID-19 infection (35.5%) when compared to the patients with the mild infection (9.9%), suggesting that early decline of SPO_2 could be an indicator for severe infection. As a marker for systemic inflammatory response, CK has been reported to be associated with higher risk of disease progressing in patients with influenza A (H1N1) viral pneumonia [42], and in patients with severe COVID-19 infection [7,9,12]. Recent studies have reported that elevated CK was commonly seen in patients with COVID-19, indicating possible damage to skeletal muscle and cardiac muscle [7–10,12]. Therefore, it was not surprising to see our model performance improved after incorporating these known factors associated with COVID-19 infection to the modeling process.

Chest CT has been frequently performed on patients with COVID-19 infection to assess pulmonary pathology. We also identified several imaging findings of COVID-19 infection such as lung consolidation, ground-glass opacity, and pulmonary infiltration, etc. However, for the purpose of CT-derived myosteatosis measurements, the chest CT scans in our study did not extend down to the L3 level per routine standard clinical imaging protocol and the L3 level has been used for assessing body composition in prior literature [22,23]. Nevertheless, all our chest CT scans included the T12 level, which should be the ideal level for assessing thoracic body composition. We therefore used the CT images at the T12 level for our study of myosteatosis in patients with COVID-19 infection.

Our study did not show diabetes as a significant predictor for transition to severe illness in our cohort of patients with COVID-19 infection. There are several potential explanations. First, our result may partly be due to our imbalanced sample size with relatively small cohort of patients in the severe illness group ($n = 31$ out of a total of 234 patients), which may have resulted in less ideal optimization of predictive modeling. Second, diabetes mellitus is a complex metabolic disease causing hyperglycemia and encompassing various aspects of insulin resistance and metabolic derangement. In this retrospective study, we did not have the data to delve into the details of diabetes for our patients such as the types of diabetes (type 1 or type 2), the duration and treatment regimen of diabetes, history of diabetic complications, etc. Instead, only limited information was abstracted from retrospective chart review as whether the patients had history of diabetes. This approach may have hindered our effort to assess the impact of confounding factors for transition to severe illness in patients with COVID-19 infection. Nevertheless, this study provided pilot data for hypothesis generating to continue our research. Our new multicenter study is underway to investigate the association between body composition and COVID-19 infection focusing on comprehensive analysis of confounding factors such as insulin resistance, diabetes, and metabolic syndrome.

The impact of body composition and metabolic derangement on disease progression cannot be underestimated. CT-derived myosteatosis parameters such as SM-RA and SMF to indicate fat infiltration in the muscle have been shown to be strongly correlated multiple factors including insulin resistance, diabetes, obesity, aging, cancer, hypertension, and cardiovascular disease [19,22–29]. Coincidentally, these factors have been reported to be relevant for severity and prognosis of COVID-19 infection [6,7,9,10,12,13]. We

speculate that myosteatosis may be a phenotype that is common for various pathological conditions such as diabetes and COVID-19 infection. The CT-derived myosteatosis parameters such as SM-RA and SMFI may be the imaging features reflecting these pathological conditions. Therefore, it should not be surprising that SM-RA and SMFI played key roles in predicting the transition risk of COVID-19 infection in our final model. Our study provided preliminary data to support the notion for potentially using the CT-derived myosteatosis parameters as imaging biomarkers of disease progression impacted by confounding factors such as diabetes in COVID-19 infection.

There were limitations to this study. First, this was a multicenter retrospective study which may make the case selection bias inevitable. We made effort to decrease this bias through adaptation of the Chinese Management Guideline for COVID-19 and enrolling all patients with the same mild common-subtype infection. Second, patients were retrospectively enrolled from six COVID-19 designated hospitals and their chest CT images were acquired from different CT scanners with varying imaging parameters. Therefore, subtle differences in CT-derived myosteatosis measurements may be present and we did not have the statistical power to consider the effect of different scanners on myosteatosis measurements. Third, although there was a relatively large number of patients with initial diagnosis of the mild common-subtype COVID-19 infection in this study, the number of cases with severe illness was still small, which may affect the performance of predictive modeling and may also affect the generalizability of our study results. Large-scale prospective multicenter study with standardized imaging protocol should be helpful to validate our results.

In summary, we found CT-derived measurements of thoracic myosteatosis to be associated with higher risk of transition to severe illness in patients affected by COVID-19 who initially presented as having the mild common-subtype infection. The myosteatosis nomogram developed in this study could potentially provide an individualized prediction of the transition risk to severe illness, thus assisting in making treatment decision for patients with COVID-19 infection in the early stage. Our study presented promising data for potential use of body composition analysis in the overall assessment of disease progression and prognosis in patients with COVID-19 infection.

Funding

This research received no external funding.

Consent for publication

Not applicable.

Author contributions

Xiaoping Yi: Conceptualization, Methodology, Original draft preparation, Investigation, Validation, Reviewing and Editing.

Haipeng Liu: Conceptualization, Methodology, Original draft preparation, Investigation, Validation, Reviewing and Editing.

Liping Zhu: Conceptualization, Methodology, Original draft preparation, Investigation, Validation, Reviewing and Editing.

DongCui Wang: Data curation, Investigation.

Fangfang Xie: Data curation, Investigation.

Linbo Shi: Data curation, Investigation.

Ji Mei: Data curation, Investigation.

Xiaolong Jiang: Data curation, Investigation.

Qiuhua Zeng: Data curation, Investigation.

Pingfeng Hu: Data curation, Investigation.

Yihui Li: Data curation, Investigation.

Peipei Pang: Methodology, Software, Visualization. Guangwu Lei: Investigation.

Jie Liu: Data curation, Investigation.

Wanxiang Peng: Data curation, Investigation.

Harrison X. Bai: Conceptualization, Methodology, Writing-Original draft preparation, Supervision, Validation, Reviewing and Editing.

Weihua Liao: Conceptualization, Methodology, Writing- Original draft preparation, Supervision, Validation, Reviewing and Editing.

Bihong T. Chen: Supervision, Methodology, Reviewing and Editing.

Conflicts of interest

The authors declare that they have no competing interests.

Acknowledgements

We thank all referring hospital staff (see Supplementary files for a full list of the participating hospitals) for their efforts in assisting data collection and analysis. We appreciate all health care workers for caring patients and fighting the COVID-19 pandemic.

Appendix A. Supplementary data

Supplementary data to this article can be found online at https://doi.org/10.1016/j.clnu.2021.05.031.

References

[1] Zhu N, Zhang D, Wang W, Li X, Yang B, Song J, et al. A novel coronavirus from patients with pneumonia in China, 2019. N Engl J Med 2020;382:727–33.

[2] Zhou P, Yang XL, Wang XG, Hu B, Zhang L, Zhang W, et al. A pneumonia outbreak associated with a new coronavirus of probable bat origin. Nature 2020;579(7798):270–3.

[3] Wu JT, Leung K, Leung GM. Nowcasting and forecasting the potential domestic and international spread of the 2019-nCoV outbreak originating in Wuhan, China: a modelling study. Lancet 2020;395(10225):689–97.

[4] Parry J. Wuhan: britons to be evacuated as scientists estimate 44 000 cases of 2019-nCOV in the city. BMJ 2020;368:m351.

[5] Li Q, Guan X, Wu P, Wang X, Zhou L, Tong Y, et al. Early transmission dynamics in wuhan, China, of novel coronavirus-infected pneumonia. N Engl J Med 2020;382:1199–207.

[6] Qiu H, Tong Z, Ma P, Hu M, Peng Z, Wu W, et al. Intensive care during the coronavirus epidemic. Intensive Care Med 2020;46:576–8.

[7] Zhou F, Yu T, Du R, Fan G, Liu Y, Liu Z, et al. Clinical course and risk factors for mortality of adult inpatients with COVID-19 in Wuhan, China: a retrospective cohort study. Lancet 2020;395:1054–62.

[8] Guan WJ, Ni ZY, Hu Y, Liang WH, Ou CQ, He JX, et al. Clinical characteristics of coronavirus disease 2019 in China. N Engl J Med 2020;382:1708–20.

[9] Chen N, Zhou M, Dong X, Qu J, Gong F, Han Y, et al. Epidemiological and clinical characteristics of 99 cases of 2019 novel coronavirus pneumonia in Wuhan, China: a descriptive study. Lancet 2020;395(10223):507–13.

[10] Huang C, Wang Y, Li X, Ren L, Zhao J, Hu Y, et al. Clinical features of patients infected with 2019 novel coronavirus in Wuhan, China. Lancet 2020;395:497–506.

[11] National Health Commission of the People's Republic of China. Chinese management guideline for COVID-19 (version 7.0). http://39.134.253.34/cache/www.nhc.gov.cn/yzygj/s7653p/202003/46c9294a7dfe4cef80dc7f5912eb1989/files/ce3e6945832a438eaae415350a8ce964.pdf?ich_args2=245-24154600065449_f32a0b9f969d8670abb9ee3d42d8e898_10001002_9c896c29d7c0f4d89e3f518939a83798_0ad7c3e0d3161a7f69a04f61b3ce861b; 2020.

[12] Wang Z, Yang B, Li Q, Wen L, Zhang R. Clinical features of 69 cases with coronavirus disease 2019 in wuhan, China. Clin Infect Dis 2020;71:769–77.

[13] Arentz M, Yim E, Klaff L, Lokhandwala S, Riedo FX, Chong M, et al. Characteristics and outcomes of 21 critically ill patients with COVID-19 in Washington state. J Am Med Assoc 2020;323:1612–4.

[14] Arabi YM, Fowler R, Hayden FG. Critical care management of adults with community-acquired severe respiratory viral infection. Intensive Care Med 2020;46(2):315–28.

[15] Bouadma L, Lescure FX, Lucet JC, Yazdanpanah Y, Timsit JF. Severe SARS-CoV-2 infections: practical considerations and management strategy for intensivists. Intensive Care Med 2020;46:579–82.
[16] Guo L, Wei D, Zhang X, Wu Y, Li Q, Zhou M, et al. Clinical features predicting mortality risk in patients with viral pneumonia: the MuLBSTA score. Front Microbiol 2019;10:2752.
[17] Chen W, Lan Y, Yuan X, Deng X, Li Y, Cai X, et al. Detectable 2019-nCoV viral RNA in blood is a strong indicator for the further clinical severity. Emerg Microb Infect 2020;9(1):469–73.
[18] Ruan Q, Yang K, Wang W, Jiang L, Song J. Clinical predictors of mortality due to COVID-19 based on an analysis of data of 150 patients from Wuhan, China. Intensive Care Med 2020;46:846–8.
[19] Gfp A, Shachar SS, Nyrop KA, Muss HB, Malpica L, Williams GR. Myosteatosis and prognosis in cancer: systematic review and meta-analysis. Crit Rev Oncol Hematol 2020;145:102839.
[20] Souza NC, Gonzalez MC, Martucci RB, Rodrigues VD, de Pinho NB, de Leon AP, et al. Frailty is associated with myosteatosis in obese patients with colorectal cancer. Clin Nutr 2020;39(2):484–91.
[21] West MA, van Dijk DPJ, Gleadowe F, Reeves T, Primrose JN, Abu HM, et al. Myosteatosis is associated with poor physical fitness in patients undergoing hepatopancreatobiliary surgery. J Cachexia Sarcopenia Muscle 2019;10(4):860–71.
[22] van der Kroft G, van Dijk DPJ, Rensen SS, Van Tiel FH, de Greef B, West M, et al. Low thoracic muscle radiation attenuation is associated with postoperative pneumonia following partial hepatectomy for colorectal metastasis. (Oxford): HPB; 2019.
[23] Martin L, Birdsell L, Macdonald N, Reiman T, Clandinin MT, McCargar LJ, et al. Cancer cachexia in the age of obesity: skeletal muscle depletion is a powerful prognostic factor, independent of body mass index. J Clin Oncol 2013;31(12):1539–47.
[24] Radovanovic D, Sotgiu G, Jankovic M, Mahesh PA, Marcos PJ, Abdalla MI, et al. An international perspective on hospitalized patients with viral community-acquired pneumonia. Eur J Intern Med 2019;60:54–70.
[25] Czigany Z, Kramp W, Bednarsch J, van der Kroft G, Boecker J, Strnad P, et al. Myosteatosis to predict inferior perioperative outcome in patients undergoing orthotopic liver transplantation. Am J Transplant 2020;20(2):493–503.
[26] Maeda K, Akagi J. Muscle mass loss is a potential predictor of 90-day mortality in older adults with aspiration pneumonia. J Am Geriatr Soc 2017;65(1):e18–22.
[27] Cruz-Jentoft AJ, Sayer AA. Sarcopenia. Lancet. 2019;393(10191):2636–46.
[28] Cesari M, Fielding RA, Pahor M, Goodpaster B, Hellerstein M, van Kan GA, et al. Biomarkers of sarcopenia in clinical trials-recommendations from the international working group on sarcopenia. J Cachexia Sarcopenia Muscle 2012;3(3):181–90.
[29] Cruz-Jentoft AJ, Baeyens JP, Bauer JM, Boirie Y, Cederholm T, Landi F, et al. Sarcopenia: European consensus on definition and diagnosis: report of the European working group on sarcopenia in older people. Age Ageing 2010;39(4):412–23.
[30] Karlsson EA, Schultz-Cherry S, Rosch JW. Protective capacity of statins during pneumonia is dependent on etiological agent and obesity. Front Cell Infect Microbiol 2018;8:41.
[31] Organization WH. Corona- virus disease (COVID-19) technical guidance: laboratory testing for 2019-nCoV in humans. https://www.who.int/emergencies/diseases/novel-coronavirus-2019/technical-guidance/laboratory-guidance.
[32] Tunes-da-Silva G, Klein JP. Cutpoint selection for discretizing a continuous covariate for generalized estimating equations. Comput Stat Data Anal 2011;55(1):226–35.
[33] Chiang PL, Chen YS, Lin AW. Altered body composition of psoas and thigh muscles in relation to frailty and severity of Parkinson's disease. Int J Environ Res Publ Health 2019;16(19).
[34] Martin L, Gioulbasanis I, Senesse P, Baracos VE. Cancer-associated malnutrition and CT-defined sarcopenia and myosteatosis are endemic in overweight and obese patients. JPEN - J Parenter Enter Nutr 2020;44(2):227–38.
[35] Green WD, Beck MA. Obesity altered T cell metabolism and the response to infection. Curr Opin Immunol 2017;46:1–7.
[36] Milner JJ, Beck MA. The impact of obesity on the immune response to infection. Proc Nutr Soc 2012;71(2):298–306.
[37] Widdicombe JG, Addington WR, Fontana GA, Stephens RE. Voluntary and reflex cough and the expiration reflex; implications for aspiration after stroke. Pulm Pharmacol Therapeut 2011;24(3):312–7.
[38] Sillanpää E, Stenroth L, Bijlsma AY, Rantanen T, McPhee JS, Maden-Wilkinson TM, et al. Associations between muscle strength, spirometric pulmonary function and mobility in healthy older adults. Age (Dordr). 2014;36(4):9667.
[39] Gray C, MacGillivray TJ, Eeley C, Stephens NA, Beggs I, Fearon KC, et al. Magnetic resonance imaging with k-means clustering objectively measures whole muscle volume compartments in sarcopenia/cancer cachexia. Clin Nutr 2011;30(1):106–11.
[40] Larsson L, Degens H, Li M, Salviati L, Lee YI, Thompson W, et al. Sarcopenia: aging-related loss of muscle mass and function. Physiol Rev 2019;99(1):427–511.
[41] Lupisan S, Suzuki A, Macalalad N, Egos R, Sombrero L, Okamoto M, et al. Etiology and epidemiology of community-acquired pneumonia in adults requiring hospital admission: a prospective study in rural Central Philippines. Int J Infect Dis 2019;80:46–53.
[42] Lobo SM, Asa W, Mlm S, Queiroz F, Gandolfi JV, de Oliveira NE, et al. Excess mortality is associated with influenza A (H1N1) in patients with severe acute respiratory illness. J Clin Virol 2019;116:62–8.